CONTAINERLESS PROCESSING OF LIQUID METALS IN MICROGRAVITY

Iván Egry

Institut für Materialphysik im Weltraum, DLR, 51170 Köln, Germany, Email: Ivan.Egry@dlr.de

ABSTRACT

This paper reviews how the microgravity environment can be used for the precise measurement of thermophysical properties of liquid metals. To take full advantage of microgravity, containerless processing techniques in combination with non-contact diagnostic tools have been applied. In some cases, such experiments are only possible in microgravity, in others microgravity improves the accuracy considerably.

1. INTRODUCTION

Materials sciences provide the basis for most modern technologies, e.g. IT and photovoltaics, aerospace and automotive applications, nano- and biotechnology, just to name a few. In recent years, the trend in developing new products moved from the conventional try-and-error approach to computer-based modelling. This has become possible due to the increase in computer power, but it is still hampered by an incomplete understanding of all mechanisms involved and by a lack of available thermophysical property data. In order to further advance the field, a multiscale and multidisciplinary approach is necessary, combining experimental and theoretical work with computer simulations on all length scales, starting from microscopic ab-initio calculations, covering the mesoscopic scale by, e.g., phase field methods, and finally simulating the finishing steps, such as near net shape casting.

Material scientists originally devoted most of their efforts to studying the solid state of materials, its microstructure and its mechanical and thermal properties. However, in the last 10 to 20 years, a change in paradigm has taken place, and the importance of the liquid phase has been recognised. In fact, almost all industrially used materials have been molten in some processing step, specifically in casting. Solidification from the melt leaves its fingerprints in the final material, and hence it is of utmost importance to understand the properties of the molten state and its solidification behaviour. The prominent feature of fluids, namely their ability to flow and to form free surfaces, poses the main difficulty in theoretically describing them. The physics of fluids is governed by the Navier-Stokes equation and by the ubiquitous presence of convection. In addition, when dealing with metallic materials, the high temperatures involved lead to experimental difficulties, the most trivial, but also most fundamental, being the availability of suitable containers. Consequently, the measurement of thermophysical properties of the liquid phase, in particular at high temperatures, is a very difficult task under terrestrial conditions.

With the advent of microgravity platforms, a new tool has become available to study the properties of fluids. In the absence of gravity, density differences play no role; consequently sedimentation effects and buyoancy driven convection can be minimised which allows to study fluids and their solidification in a quiescent environment. A number of fundamental and seminal microgravity experiments have been performed since then, sheding new light onto old problems and, in some cases, rendering accepted textbook knowledge erroneous. An important breakthrough was the application of containerless processing techniques in the microgravity environment, which gave access to the metastable region of an undercooled melt and allowed measurements of growth velocities as function of undercooling, leading to a revision of dendrite growth and grain refining theories. In addition, containerless processing using electromagnetic levitation solved the problem of finding a suitable container for high-temperature, highly reactive metallic melts and allowed to measure thermophysical properties of these melts with a high precision.

2. MICROGRAVITY

Microgravity is the term commonly used to describe weightlessness conditions onboard a spacecraft. Unfortunately, this term is quite misleading: first of all, gravity remains essentially unaltered, i.e. the strength of the gravity field 300 km above the surface of the earth is still about 90% of its sea-level value. Second, the apparent weight is typically reduced by a factor of 10^3, rather than 10^6.

The physical origin for weightlessness lies in the fact that the experiments are carried out in a frame of reference which is accelerated with respect to an inertial frame. Consequently, Newton's equations of motion have to be supplemented by a fictitious force:

$$F_s = -m\ddot{s}\,, \qquad (1)$$

where $\ddot{s}$ is the acceleration of the frame of reference along its trajectory, *s*, with respect to an inertial system (e.g. the earth.)

Proc. '19th ESA Symposium on European Rocket and Balloon Programmes and Related Research, Bad Reichenhall, Germany, 7–11 June 2009 (ESA SP-671, September 2009)

For a circular motion with angular frequency ω and radius R, like an orbiting satellite, this force is the centrifugal force:

$$F_c = m\omega^2 R \qquad (2)$$

For trajectories close to the earth's surface the gravitational acceleration can be assumed constant in magnitude and direction. In this case, $F_s = mg$, and a parabolic trajectory follows. For the trajectories of sounding rockets with an apogee of more than 200 km, this approximation is no longer justified. In fact, a sounding rocket flies along an elliptical path.

If the fictitious force cancels the gravitational force, there is no net force on the body, it is weightless. In reality, a complete cancellation of the forces cannot be achieved, due to the spatial dependence of the earth's gravitational field (tidal forces), the still existing air drag, and internal disturbances within the spacecraft (g-jitter). Weightlessness conditions can be achieved in drop tubes or drop towers, in parabolic flights, onboard sounding rockets, and on orbiting spacecrafts like the International Space Station ISS. Whereas tidal forces are negligible for sounding rocket missions due to the small size of the payload, the major residual acceleration stems from an incomplete de-spin of the rocket's original rotation.

Table 1 shows the characteristics of the main facilities for microgravity studies available today, including the time interval available for a given measurement.

	g level, g_0	*μg duration, s*	*payload volume, m^3*
Drop tower	$10^{-3} - 10^{-6}$	1 – 10	≈ 0.1
Aircraft	$10^{-2} - 10^{-3}$	≈20	≈ 1.0
Sounding rocket	$10^{-4} - 10^{-6}$	100 – 1000	≈ 0.1
Space Station	$10^{-3} - 10^{-6}$	∞	≈ 1.0

Table 1. Available microgravity platforms.

The available free-fall time in a drop tube/drop tower scales with the square root of its height. It can be doubled if the payload is shot vertically upwards from the bottom of the tower, instead of dropping it from its top. This technically challenging catapult mode of operation has recently been introduced at the drop tower of ZARM in Bremen. An aircraft on a parabolic trajectory can provide a reduced gravity environment for about 20 seconds per parabola. Usually, up to 40 consecutive parabolas are performed per flight. Sounding rockets can provide free-fall periods betwen 5 and 20 minutes. As an example the experiment protocol for a CuCo sample processed in an electromagnetic levitation facility onboard a TEXUS sounding rocket is shown in Figure 1. The experiment time is restricted to about 120 s, since two such experiments have to be carried out during one mission.

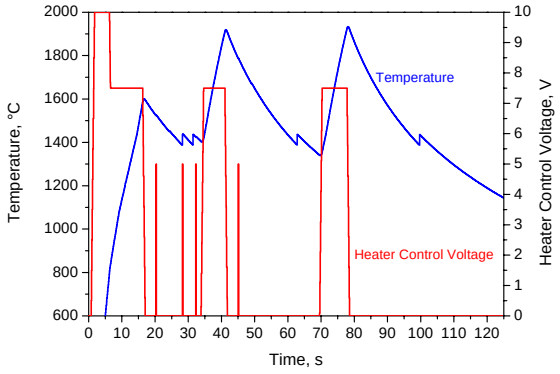

Figure 1. Temperature (left), heating and positioning control voltage(right) as function of time for containerless processing of a Cu-Co sample during a TEXUS sounding rocket flight.

Liquids are the most sensitive of the phases to a gravitational force. This force causes an acceleration of all masses towards the center of gravitation, and it makes bodies fall and fluids flow downwards. In an inhomogeneous fluid system at rest, sedimentation will result. In addition, gravity can also induce flows in combination with a temperature or concentration gradient. This is called buoyancy driven convection and can lead to fluid flow instabilities, like the Rayleigh-Bénard instability [1]. Consequently, in the absence of gravity, none of these effects will occur. Specifically, this means that

- no container is needed for positioning a fluid
- there is no sedimentation
- there is no buoyancy driven convection.

In the absence of gravity, surface tension becomes the dominant force for a liquid system. It holds a liquid drop together and controls its wetting behaviour. Therefore, capillarity phenomena become important in microgravity conditions. Variations in temperature or concentration along a free surface induce variations in the local surface tension, leading to surface tension driven convection. This effect was discovered by Marangoni [2] and is named after him. In other words, Marangoni convection replaces the buoyancy driven Rayleigh-Bénard convection in microgravity. The absence of gravity therefore does not imply the absence of convection.

3. CONTAINERLESS METHODS

Thermophysical properties of high temperature, and highly reactive, melts can be conveniently measured by containerless methods. These methods provide the

purest environment possible. Since the surface of the liquid sample is not in contact with a wall, Marangoni convection will occur, if there is a temperature or concentration gradient along the surface.

There are a number of containerless processing techniques, based on different levitation fields [3]. Acoustic and aerodynamic levitation techniques use standing waves or pressure gradients of a carrier gas, respectively. In electrostatic levitation, an electrostatic field is used to position a charged or polarized sample. In diamagnetic levitation, the molecular magnetic moments couple to an external dc magnetic field of typically 1-5 T. Electromagnetic levitation uses high frequency electromagnetic fields and exploits the Lorentz force to levitate electrically conducting specimen. Except for the latter, all other methods require an independent heating system in order to melt the sample, usually an infrared laser. Although there have been some early attempts to operate different levitators under microgravity conditions, up to date the only successful implementation of a microgravity levitator is TEMPUS [4, 5], based on the electromagnetic levitation principle. Thermophysical properties of levitated samples have been measured in TEMPUS during two Spacelab missions, IML-2 in 1994 [6] and MSL-1 in 1997 [7]. Later on, TEMPUS was flown regularly on parabolic flight campaigns. Its successor, MSL-EML, was flown in 2006 and 2008 on a sounding rocket, and is presently being built as a second generation payload for ISS, to be flown in 2011.

In the following, the principle of electromagnetic levitation is briefly described. Levitation of electrically conducting samples is achieved by placing the sample into a high frequency alternating inhomogeneous electromagnetic field, produced by a levitation coil with a conical or cylindrical shape. This field B induces a current in the sample which, in turn, interacts with the field. Levitation is caused by the Lorentz force, F. Its magnitude can be expressed, to lowest order in a multipole expansion [8], as:

$$F_L = -\frac{\nabla B^2}{2\mu_0}\frac{4\pi}{3}a_0^3 Q(q) \qquad (3)$$

where μ_0 is the magnetic permeability, a_0 is the radius of the sample, $q=a_0/\delta$ is a dimensionless quantity and δ is the skin depth, defined as follows:

$$1/\delta = \sqrt{\frac{\omega\,\sigma\,\mu_0}{2}} \qquad (4)$$

Here, σ is the electrical conductivity of the sample, and ω is the frequency of the alternating field. The function $Q(q)$ is given by:

$$Q(q) = \frac{3}{4}\left(1 - \frac{3}{2q}\frac{\sinh(2q)-\sin(2q)}{\cosh(2q)-\cos(2q)}\right) \qquad (5)$$

For stable levitation, this field has to cancel the gravitational field:

$$\vec{F}_L = -\vec{F}_g = -\frac{4\pi}{3}a_0^3\rho\vec{g} \qquad (6)$$

Here, ρ is the density of the sample, and g is the gravity vector. For a linear magnetic field, the levitation force is given by [9]:

$$F_L = 2\pi a_0^3 z_0 \mu_0 H_{zz}^2 \qquad (7)$$

where H_{zz} is the derivative of the z-component of the field with respect to z, and z_0 is the equilibrium position of the droplet, measured downwards from the origin of the magnetic field, i.e. from the equatorial plane of the coil.

In contrast to other levitation techniques, electromagnetic levitation is intrinsically stable, i.e. there is a restoring force for deviations from the equilibrium position in any direction. Consequently, a solid sample performs oscillations about its equilibrium position with a frequency which is determined by the "spring constant" of the field, and its mass. For the magnetic field introduced above, this frequency can be calculated and is given by [9]:

$$\Omega_{\parallel}^2 = \frac{3\mu_0}{2\rho}H_{zz}^2, \qquad \Omega_{\perp}^2 = \frac{1}{4}\Omega_{\parallel}^2 \qquad (8)$$

where $\Omega_{\parallel}^2$ is the frequency for oscillations along the symmetry axis, and $\Omega_{\perp}^2$ is the frequency for oscillations in a plane perpendicular to it.

In addition, the sample may also rotate along any axis which, for a liquid sample, leads to a flattening and eventual fission of the drop, due to the centrifugal forces. This kind of instability is often encountered in practice, and has been studied theoretically by Gerbeth and coworkers [10, 11].

Under terrestrial conditions, the joint action of the gravitational and levitation force leads to a deformation of a liquid sample: the drop is elongated along the z-axis, i.e. the direction of the gravity vector. As will be seen later, such a deformation is detrimental to thermophysical property measurements. On the other hand, the liquid sample remains essentially spherical in microgravity.

In addition, electromagnetic fields induce fluid flows inside a liquid, conducting body. The calculation of the corresoponding flow pattern is a formidable task for magnetohydrodynamic calculations [12]. In particular,

if these fields become turbulent, they render the measurement of viscosity impossible. This can only be avoided in microgravity, where only small positioning fields are required.

Electromagnetic levitation not only provides positioning, it also enables inductive heating of the levitated sample. The power P absorbed by the sample due to ohmic losses of the induced currents is given by [13]:

$$P = \frac{B^2}{2\mu_0}\omega\frac{4\pi}{3}a_0^3 H(q) \qquad (9)$$

with $H(q)$ defined as:

$$H(q) = \frac{9}{4q^2}\left(q\frac{\sinh(2q)+\sin(2q)}{\cosh(2q)-\cos(2q)}-1\right) \qquad (10)$$

The functions $Q(q)$ and $H(q)$ are shown in Figure 2.

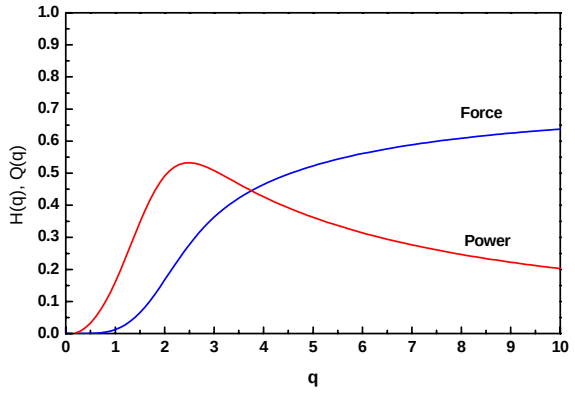

Figure 2. Heating and positioning efficiencies of electromagnetic levitation.

4. MICROGRAVITY EXPERIMENTS

The measurement of thermophysical properties of liquid metals using electromagnetic levitation has become a routine task in the past few years, at least concerning surface tension and density measurements, and comprehensive reviews are available [14, 15, 16]. Concerning experiments under microgravity, the major event was the Spacelab mission MSL-1 in 1997 [7]. Since then, no long-duration microgravity campaign has taken place. However, a number of parabolic flights using electromagnetic levitation has been performed, and also two sounding rocket flights. In the following, we will concentrate on results obtained during the TEXUS missions TEXUS 42 and TEXUS 44.

4.1. Specific Heat

A non-contact method developed by Fecht and Johnson [17] can be used to determine the specific heat in levitation experiments. It is a variant of non-contact modulation calorimetry, normally used in low temperature physics. The heater power is modulated according to $P_\omega(t) = \Delta P_\omega \cos(\omega t)$ resulting in a modulated temperature response ΔT_ω of the sample. A thermal model considering heat loss to the environment and heat conduction within the sample has been developed by Wunderlich [18]. It considers heat loss to the exterior (typically by radiation only if the experiment is carried out under vacuum), spatially inhomogeneous heating of the sample, and heat conduction within the sample. For small Biot numbers, $Bi = k_r/k_c << 1$, where k_r is the heat loss due to radiation and k_c the heat loss due to heat conduction, adiabatic conditions are realized and quantitative modulation calorimetry is possible. Under such conditions, the following relation for ΔT_ω is obtained:

$$\Delta T_\omega = \frac{\Delta P_\omega}{\omega c_p}\left\{\left(1+\left(\frac{\omega}{\lambda_1}\right)^2\right)\left(1+\left(\frac{\lambda_2}{\omega}\right)^2\right)\right\}^{-1/2} \qquad (11)$$

where λ_1 and λ_2 are functions of k_r and k_c such that for $Bi << 1$, $\lambda_2 << \lambda_1$. This allows to choose the modulation frequency between λ_2 and λ_1 such that $\lambda_2 << \omega << \lambda_1$. Under these circumstances, a simple relation for the the specific heat, c_p, can be derived:

$$c_p = \frac{1}{\omega}\frac{\Delta P_\omega}{\Delta T_\omega} \qquad (12)$$

The power input into the sample, ΔP_ω, cannot be measured directly. It is related to the current I flowing through the heating coil by a coupling coefficient G_H which has to be determined separately:

$$\Delta P_\omega = G_H I_\omega^2 \qquad (13)$$

It should be noted that a harmonic modulation of the current with ω' leads to components in the power P with $\omega = 0$, $\omega = \omega$' and $\omega = 2\omega$'. The static and frequency-doubled components can also be analyzed along the lines indicated above.

Modulation calorimetry needs to be carried out under isothermal conditions, i.e. the sample must be allowed to thermalize at a predefined temperature before the modulation signal can be applied. Therefore, such experiments cannot be performed during parabolic flights. Fecht and coworkers [19] applied this method during the MSL-1 Spacelab mission. The temperature modulation is shown in Figure 3, where the quaternary alloy $Zr_{65}Al_{7.5}Cu_{17.5}Ni_{10}$ was undercooled by 194 K, and

modulation calorimetery could be performed in the equilibrium as well as in the undercooled liquid. More recently, Wunderlich *et al.* performed modulation calorimetry during TEXUS 42 on a $Ti_{46}Al_{46}Nb_8$ alloy in the framework of the IMPRESS project [20]. It was possible to determine both, the specific heat, and the total hemispherical emissivity in the liquid phase [21]. The results are shown in Table 2.

T / °C	1570	1491	1468
c_P / J K^{-1} g^{-1}	1.14	1.06	1.03
ε_{tot}	0.44	0.36	0.34

Table 2: $Ti_{46}Al_{46}Nb_8$ specific heat capacity and total hemispherical emissivity in the liquid phase.

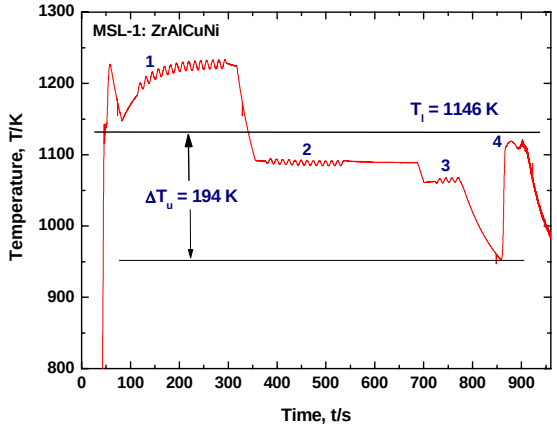

Figure 3. Modulation calorimetry on ZrAlCuNi alloy during MSL-1 Spacelab mission. The melting temperature of this alloy is 1146 K. Modulation was carried out in the equilibrium liquid (1), as well as in the undercooled liquid (2,3). At point 4, solidification occurs from an undercooling level of 194 K.

4.2. Surface tension

Surface tension of levitated samples is conveniently measured by the oscillating drop technique [22]. Liquid samples perform oscillations around their equilibrium shape. In microgravity, this is a sphere and in that case, a simple formula can be used to relate the frequency ω of the oscillations to the surface tension γ. The so-called Rayleigh frequency is given by:

$$\omega_R^2 = \frac{32\pi}{3}\frac{\gamma}{M} \qquad (14)$$

where M is the mass of the droplet and a_0 its radius. Depending on the sample mass, typical frequencies $\nu = \omega/2\pi$ lie in the range of 30 – 50 Hz.

Under terrestrial conditions, the liquid drop is distorted by gravity and the compensating levitation field. As a consequence, the single frequency is split into up to 5 peaks. In addition, all peaks are shifted with respect to eqn (14). This is due to the fact that the electromagnetic levitation field acts as an additional pressure term in the Navier-Stokes equation. It therefore leads to an apparent increase in surface tension. A correction formula to account for these effects on the frequency spectrum was developed by Cummings and Blackburn [9] who derived a sum rule which contains only measurable frequencies. It reads:

$$\frac{32\pi}{3}\frac{\gamma}{M} = \frac{1}{5}\sum_m \omega_{2,m}^2 - 1.9\,\overline{\Omega_{tr}^2} - 0.3\,(\overline{\Omega_{tr}^2})^{-1}\,(g/a_0)^2 \qquad (15)$$

Here $\overline{\Omega_{tr}^2}$ is the mean translational frequency of the drop, a_0 its radius and g is the gravitational acceleration.

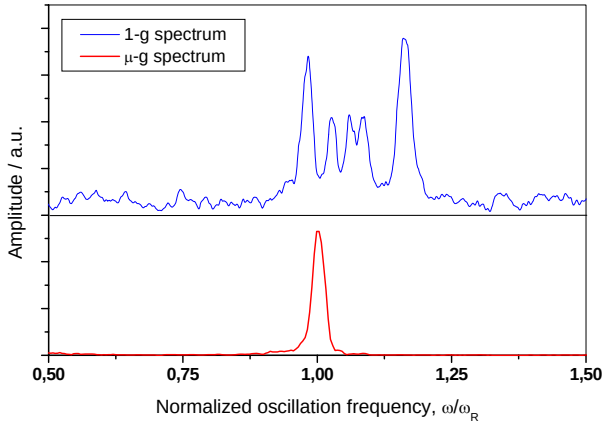

Figure 4. Frequency spectrum of an oscillating AuCu drop under 1g (top) and microgravity (bottom)

The sample oscillations are recorded with video cameras from the top, i.e. along the symmetry axis. The frame rate must satisfy the Nyquist theorem to avoid aliasing and is typically 100 – 400 fps. The area of the cross section of the sample, its center of mass, and two perpendicular radii are calculated for each frame. A number of frames is taken and the corresponding time series is Fourier transformed to yield the frequencies. From the time dependence of the center of mass the translational frequencies are derived, whereas the surface oscillation frequencies are contained in the temporal behaviour of the two perpendicular radii. Due to their different symmetries, the oscillations corresponding to different m-values can be identified using selection rules, as derived by Egry *et al.* [22].

In Figure 6, oscillation spectra of a gold-copper alloy are shown, recorded on ground and in microgravity during the IML-2 Spacelab mission [23]. As can be seen in the ground-based spectra, both, a splitting of the

single frequency into 5 peaks, and a shift to higher frequencies occur.

By comparing measurements in microgravity with ground-based results, the validity of the Cummings correction has been confirmed experimentally. It is fair to say that this benchmark experiment under microgravity has led to a calibration of the ground-based measurements applying the oscillating drop technique, which has consequently become the accepted method for surface tension measurements of high-temperature liquid metals.

In the recent TEXUS 44 mission, Wunderlich performed surface tension measurements on Raney-nickel, a Al-50 wt%Ni alloy as function of temperature. The data gathered during two melting cycles show little scatter and can be fitted by the linear relation:

$$\gamma(T) = 1.012 - 2.86\ 10^{-4}\ (T - 1620\ K)\ \ Nm^{-1} \qquad (16)$$

This is shown in Figure 5 below.

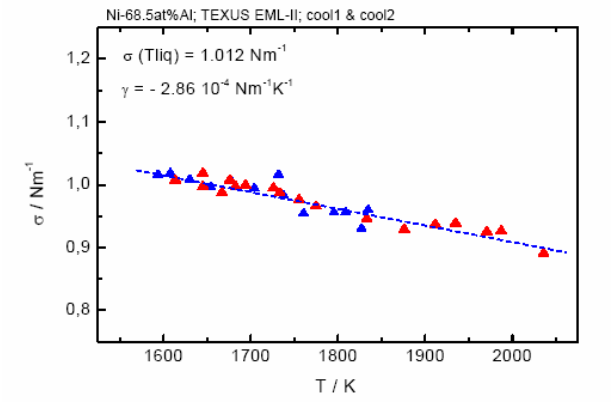

Figure 5. Surface tension of Raney-nickel as function of temperature, measured on board TEXUS 44 during two melt cycles.

4.3. Interfacial Tension

Alloys which have immiscible liquid phases have a great potential for applications. A model system for this kind of alloys is copper-cobalt: it displays a metastable miscibilty gap, accessible by a moderate undercooling of $\Delta T \approx 100$ K. This means that the liquid must be undercooled into the metastable region below its freezing point before demixing can be observed.

A levitated drop of radius R_0 consisting of two immiscible liquid phases is composed of a liquid core of radius R_i, encapsulated by the second liquid. Such a configuration can only be realised under microgravity conditions: in terrestrial levitation, the strong levitation field prohibits liquid phase separation. The oscillation spectrum of such a two-phase drop is determined by the surface tension γ of the outer liquid and the interfacial tension γ_{12} between the two liquids. Therefore, the analysis of these spectra allows the measurement of these two quantities, in particular of the interfacial tension between two immiscible liquid metals, which is otherwise hardly possible.

The oscillation spectrum of such a compound drop has been worked out [24]. To lowest order, a new frequency branch appears approximately at

$$\omega_-^2 = \frac{32\pi}{3}\frac{\gamma_{12}}{M_i} \qquad (17)$$

where M_i is the mass of the inner drop. In addition, the Rayleigh frequency is shifted upwards, resulting in a frequency shift of

$$\omega_+^2 - \omega_R^2 = \omega_R^2 \frac{\gamma_{12}}{\gamma}\left(\frac{R_i}{R_0}\right)^2 \qquad (18)$$

During the TEXUS 44 mission, a $Cu_{75}Co_{25}$ alloy was investigated. For the phase-separated sample, both, a small peak at 15 Hz, corresponding to ω_-, and the frequency shift of the Rayleigh frequency from 28 Hz to 29 Hz were observed experimentally, as shown in Figure 6 [25]. From the measured frequencies, the surface and interface tension values could be determined as follows:

$$\gamma(T) = 1.29 - 2.7710^{-4}\,(T - 1630\,K)\ Nm^{-1} \qquad (19)$$

$$\gamma_{12} = 0.17\ Nm^{-1} \qquad (20)$$

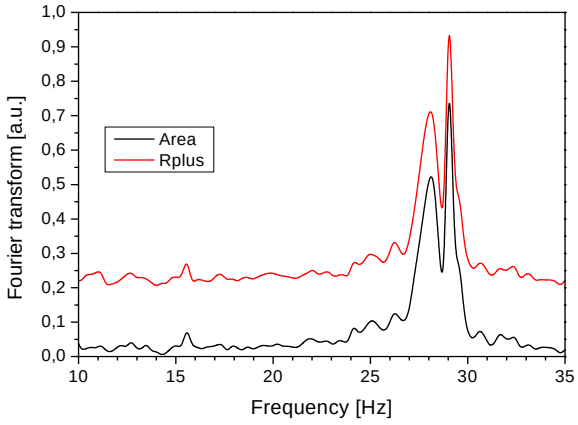

Figure 6. Oscillation spectra of a liquid $Cu_{75}Co_{25}$ drop,measured on board TEXUS 44. The broad peak at 28 Hz corresponds to the homogeneous single-phase drop, while the small peak at 15 Hz and the sharp peak at 29 Hz correspond to the demixed, two-phase drop.

4.4. Growth Velocity

A liquid (metal) can be undercooled below its freezing point, provided nucleation is sufficiently delayed. This

is the case in containerless processing by electromagnetic levitation, where the effect of container walls as potential nucleation sites is eliminated. Deep undercoolings by more than 300 K are easily attainable. When solidification eventually sets in, the growth velocity, i.e. the velocity of the solid-liquid interface can be measured as a function of undercooling by observing the moving solidification front by a high-speed camera. For moderate undercoolings, these velocities are in the range of 0.1 – 1 m/s, which means that a levitated sample solidifies in about 0.01 – 0.1 seconds. Classical dendrite growth theory [26] takes into account mass and heat transfer away from the solid-liquid interface and predicts an increase of growth velocity with undercooling. Convective effects are neglected. As shown in Figure 7, terrestrial measurements on the Raney-nickel alloy have shown the opposite trend: a decrease of growth velocity with increasing undercooling. In contrast, the measurements performed by Herlach *et al.* [27] during TEXUS 44 under microgravity conditions show much smaller undercoolings and the expected increase of growth velocity with undercooling. This striking result is as yet not understood and requires further investigations.

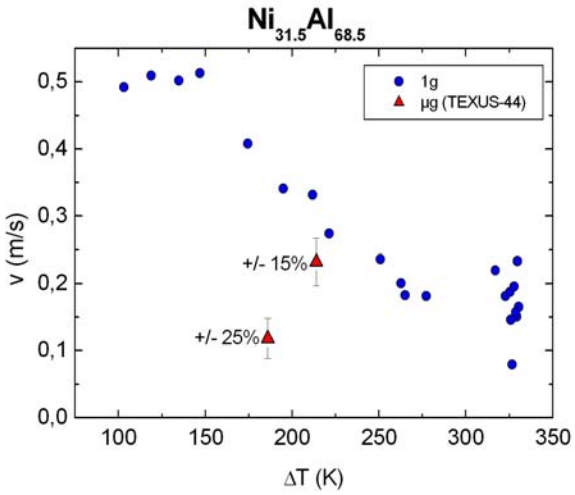

Figure 7. Solidification velocity of undercooled Raney-nickel, measured under 1g (dots) and under microgravity on board TEXUS 44 (triangles).

5. SUMMARY AND OUTLOOK

In the preceding sections, we have demonstrated the potential of the combined use of the microgravity environment and containerless processing, in particular electromagnetic levitation, for thermophysical property measurements. Due to the lack of flight opportunities, this potential has not been fully exploited yet. MSL-EML, the Materials Science Lab – Electro-Magnetic Levitator, has still to be built and will not become available before 2011. Until then, most measurements have to be carried out on board parabolic flights within 20 s of microgravity. This restricts the use of TEMPUS to surface tension and growth velocity measurements, as discussed before. For most other properties, the available microgravity period is not sufficient. Using sounding rockets as a microgravity platform is attractive in terms of microgravity duration (about 5 minutes) and also in terms of microgravity quality (about 10^{-5} g_0). However, there is only one flight every two years at best within the national German program which is co-financed by and shared with ESA. Due to restrictions in payload mass and the available µg-time, only 2 samples can be processed, yielding about 120 s experiment time per sample, as shown, e.g., in Figure 1.

When the MSL-EML on ISS becomes fully operational, experiment time will be virtually unlimited. This is the chance for performing systematic investigations varying the process parameters like, e.g., temperature, cooling and heating rates, and composition of the ambient atmosphere, i.e. the oxygen partial pressure. Generally speaking, the emphasis will shift from technology development to exploiting the technology for measurements of industrially and scientifically interesting (multicomponent) alloys. Even in this optimistic scenario, microgravity experiments will not replace a sound, ground-based measurement program. Microgravity experiments provide benchmarks for terrestrial measurements owing to their inherent higher precision. However, the huge amount of data required for numerical modelling of industrial processes by far exceeds the capabilities of spaceborne experiments.

ACKNOWLEDGEMENTS

This review is the result of continuous discusions with many colleagues involved in microgravity experiments, during the Spacelab missions, parabolic flights, or sounding rocket campaigns. Their fruitful comments are gratefully acknowledged.

REFERENCES

1. Lord Rayleigh, Phil. Mag. 32 (1916), 529-546
2. C. Marangoni: Nuovo Cim. 3 (1878) 97-115
3. D. Herlach, R. Cochrane, I. Egry, H. Fecht, L. Greer, Int. Mat. Rev. 38 (1993), 273
4. G. Lohöfer, P. Neuhaus, I. Egry, High Temperatures – High Pressures, 23, (1991) 333
5. J. Piller, A. Seidel, M. Stauber, W. Dreier, in: *Solidification 1999*, W. Hofmeister, J. Rogers, N. Singh, S. Marsh, P. Vorhees, eds., (Warrendale: TMS, 1999) p.3
6. Team TEMPUS, in: *Materials and Fluids under low Gravity*, L. Ratke, H. Walter, B. Feuerbacher, eds., (Berlin: Springer, 1996)

7. *Solidification 1999*, W. Hofmeister, J. Rogers, N. Singh, S. Marsh, P. Vorhees, eds., (Warrendale: TMS, 1999)

8. G. Lohöfer, Quarterly Appl. Math, 11 (1993) 495.

9. D. Cummings, D. Blackburn: J. Fluid Mech. 224 (1991) 395.

10. J. Priede, G. Gerbeth, IEEE Transactions on Magnetics, 36 (2000) 349.

11. J. Priede, G. Gerbeth, IEEE Transactions on Magnetics, 36 (2000) 354.

12. R.W. Hyers, Meas. Sci. Tech. 16 (2005), 394

13. G. Lohöfer, SIAM J. Appl. Math., 49 (1989) 567.

14. Ivan Egry, C. Nieto de Castro, in: *Chemical Thermodynamics*, T. Letcher ed., Blackwell, Oxford, 1999, p.171

15. H. Suga, G. Pottlacher, I. Egry, , in: *Measurement of the Thermophysical Properties of Single Phases, Experimental Thermodynamics, Volume VI*, A. Goodwin, K. Marsh, W. Wakeham.eds., Elsevier, Amsterdam, 2003, pp. 475-536

16. J. Brillo, G. Lohöfer, F. Schmidt-Hohagen, S. Schneider, I. Egry, Int. J. Mat. & Product Technology, 26, (2006), 247-273

17. H. Fecht and W. Johnson: Rev. Sci. Instr. 62 (1991) 1299

18. R.Wunderlich, H. Fecht, Meas. Sci. Tech. 16 (2005), 402

19. R. Wunderlich, R. Sagel, Ch. Ettel, H.-J. Fecht, D. Lee, S. Glade, W. Johnson, in: *Solidification 1999*, W. Hofmeister, J. Rogers, N. Singh, S. Marsh, P. Vorhees, eds., (Warrendale: TMS, 1999), 53

20. D. Jarvis, *Mater. World,* August 2005, p.11

21. R. Wunderlich, private communication

22. S. Sauerland, K. Eckler, I. Egry: J. Mat. Sci. Letters 11 (1992) 330

23. I. Egry, G. Lohöfer, G. Jacobs: Phys. Rev. Letts. 75 (1995) 4043

24. I. Egry, Z.Metallkde., 93, (2002), 528

25. I. Egry, L. Ratke, M. Kolbe, D. Chatain, S. Curiotto, L. Battezzati, E. Johnson, N. Pryds J. Mat. Sci, (2009),accepted

26. J. Christian, *The Theory of transformation in metals and alloys*, Pergamon Press, Oxford, 1975

27. D. Herlach, R.Lengsdorf, P. Galenko, H. Hartmann, C. Gandin, S. Mosbah, A. Garcia-Escorial, H. Henein, H., Adv. Eng. Mat., 10 (2008).